Automatica 61 (2015) 289–301

Contents lists available at ScienceDirect

Automatica

journal homepage: www.elsevier.com/locate/automatica

Mechanics, control and internal dynamics of quadrotor tool operation☆

Hai-Nguyen Nguyen, ChangSu Ha, Dongjun Lee

Department of Mechanical & Aerospace Engineering and IAMD, Seoul National University, Seoul, 151-744, Republic of Korea

ARTICLE INFO

Article history:
Received 1 March 2014
Received in revised form
10 April 2015
Accepted 8 August 2015

Keywords:
Aerial manipulation
Finite-time escape
Internal dynamics
Quadrotor
Tool operation
Under-actuation

ABSTRACT

We propose a novel control framework to enable a quadrotor to operate a tool attached on it. We first show that any Cartesian control at the tool-tip can be generated if and only if the tool-tip is located strictly above or below the quadrotor's center-of-mass. We then fully characterize the internal dynamics of the spatial quadrotor tool operation, which arises due to the quadrotor's under-actuation, and elucidate a seemingly counter-intuitive necessary condition for the internal stability, that is, the tool-tip should be located above the quadrotor's center-of-mass. We further manifest that this internal dynamics can exhibit finite-time escape and propose a stabilizing action to prevent that. The theory is then illustrated for the problems of rotating tool operation and hybrid force/position control with relevant simulation results.

1. Introduction

With the recent advances in sensors, actuators, materials, computing and control technologies, quadrotor-type unmanned aerial vehicles (UAVs) have gained ability to realize many useful applications such as aerial photography and movie shooting, landscape survey, surveillance and reconnaissance, search of areas after disaster, to name just few. Due to this ability and promise, the quadrotor has been the focus of attention from research community and general public alike.

Numerous successful control techniques have been proposed for the *motion control* of the quadrotor's center-of-mass position: trajectory tracking control (e.g., Aguiar & Hespanha, 2007, Frazzoli, Dahleh, & Feron, 2000, Ha, Zuo, Choi, & Lee, 2014 and Hua, Hamel, Morin, & Samson, 2009), formation control (e.g., Abdessameud & Tayebi, 2010, Lee, 2012 and Turpin, Michael, & Kumar, 2012), teleoperation (e.g., Franchi, Secchi, Son, Bulthoff, & Robuffo, 2012, Ha et al., 2014 and Lee et al., 2013), and even acrobatic flying (e.g., Mellinger, Michael, & Kumar, 2012 and Purwin & D'Andrea, 2009).

Different from these motion control results, the main concern of the current paper is *aerial manipulation*, an ability crucial to make the quadrotor truly a versatile aerial robotic platform. We particularly focus on the case where the quadrotor operates a simple rigid tool attached on it (e.g., screw-driver, contact probe, etc.) acting itself as the actuator for the tool. See Fig. 1. We envision this quadrotor-tool system to be useful for such applications as inspection and repair of remote infrastructure, operation on high-rise building exteriors, etc. We also believe this usage of simple tool would be more promising at least for some application than using a multi-link actuated robotic arm (with motors) attached to the quadrotor (e.g., Ghadiok, Goldin, & Ren, 2012, Korpela, Orsag, Oh, & Pekala, 2013 and Yang & Lee, 2014), given the limited payload of typical quadrotor platforms.

The problem of quadrotor tool operation control, however, turns out to be much more challenging than that of the motion control of the quadrotor, as a proper tool control (e.g., tool-tip position $y \in \Re^3$ of Fig. 1) would require simultaneous control of both the translation and rotation of the quadrotor, which, yet, is under-actuated only with four control inputs. More specifically, in this paper, we first show that we can generate any Cartesian control action at the tool-tip y, if and only if this tool-tip y is located either strictly above or strictly below the quadrotor's center-of-mass $x \in \Re^3$ (i.e., $d_3 \neq 0$—see Fig. 1). We then reveal that, due to

☆ Research supported in part by the Basic Science Research Program of the National Research Foundation (NRF) by the Korea Government (MEST) (2012-R1A2A2A0-1015797) and by the Global Frontier R&D Program on "Human-centered Interaction for Coexistence" of the NRF of Korea funded by MEST (NRF-2013M3A6A3079227). The material in this paper was partially presented at the ASME Dynamic Systems & Control Conference, October 17–19, 2012, Fort Lauderdale, FL, USA and at the IEEE/RSJ International Conference on Intelligent Robots and Systems, November 3–8, 2013, Tokyo, Japan. This paper was recommended for publication in revised form by Associate Editor Marco Lovera under the direction of Editor Toshiharu Sugie..

E-mail addresses: hainguyen@snu.ac.kr (H.-N. Nguyen), changsuha@snu.ac.kr (C. Ha), djlee@snu.ac.kr (D. Lee).

http://dx.doi.org/10.1016/j.automatica.2015.08.015
0005-1098/

the quadrotor's under-actuation, this Cartesian control generation gives a rise to four-dimensional internal dynamics (Sepulchre, Jankovic, & Kokotovic, 1997; Slotine & Li, 1991) and elucidate a seemingly counter-intuitive necessary condition for its stability, that is, the tool-tip y should be installed *above* the quadrotor's center-of-mass x (i.e., $d_3 < 0$—see Fig. 1), and not below it as would likely be attempted and designed in practice. We further manifest that this internal dynamics can even exhibit finite-time escape (Sepulchre et al., 1997) due to some quadratic terms therein and propose a stabilizing control action to prevent finite-time escape thereof. Finally, relying on this theoretical finding, we propose novel control laws for the two perhaps practically most important tool operation tasks: rotating tool operation (i.e., screw-driver and vertical jack) and hybrid position/force control against a working surface.

In contrast to the plethora of quadrotor motion control results as mentioned above, that for the quadrotor aerial manipulation are much fewer. Among them, we believe the followings are the most related ones to our result in this paper.

The issue of stability with perturbed/changing center-of-mass (e.g., with payload) was considered in Palunko and Fierro (2011) and Pounds, Bersak, and Dollar (2012). These results, however, were limited only to the stabilization problem (e.g., stability of the linearized planar dynamics under the PID-stabilization Pounds et al., 2012; different output than ours, which produces different and always stable internal dynamics Palunko & Fierro, 2011), and not applicable to our problem of spatial quadrotor-tool operation, where we not only need to achieve the quadrotor stability but also to drive the tool in the three-dimensional space by recruiting the quadrotor's translation and rotation motions.

In Brescianini, Hehn, and D'Andrea (2013) and Hehn and D'Andrea (2011), the authors considered the problem of a quadrotor manipulating a pole and two quadrotors achieving airborne-transfer of a pole between them. For this, they assumed that the pole motion is coupled only to the quadrotor center-of-mass position x, not to its rotation $R \in \mathrm{SO}(3)$, and also the control inputs are the quadrotor's thrust force $\lambda \in \Re$ and its angular rate $w \in \Re^3$. This in fact is in a stark contrast to our result here, where the quadrotor's rotation R must be recruited on top of its translation x to properly operate the tool, and the internal dynamics, which may exhibit even finite-time escape, arises with the angular torque input $\tau \in \Re^3$.

Hybrid position/force control problem was studied for the quadrotor (Bellens, De Schutter, & Bruyninckx, 2012; Darivianakis, Alexis, Burri, & Siegwart, 2014) and for the ducted-fan UAV (Marconi & Naldi, 2012), where, however, the quadrotor system was modeled only as a quasi-static "black box" wrench generator (Bellens et al., 2012) or simplified as a combination of the decoupled linearized north-pitch, east-roll, and down dynamics (Darivianakis et al., 2014); or the dynamics of the ducted-fan UAV was again restricted to the saggital plane and further linearized (Marconi & Naldi, 2012). Therefore, the complex (and potentially unstable) nonlinear and spatial dynamics of the quadrotor-tool operation (e.g., quadratic terms possibly triggering finite-time escape, and control action to prevent that by using pitch–roll–yaw coupling) could be neither revealed nor addressed in those works.

Another line of relevant research is Hauser, Sastry, and Meyer (1992); Martin, Devasia, and Paden (1996), where the authors obtained similar internal dynamics and condition for its stability as ours for PVTOL (planar vertical take-off and landing) systems. These results (Hauser et al., 1992; Martin et al., 1996), however, (1) were limited only to the planar dynamics, whose extension to the spatial operation not only requires substantial development as done in this paper (from the planar result of Lee & Ha, 2012) but also turns out necessary for us to design the control action to prevent finite-time escape; (2) overlooked the issue of finite-time escape, which, different from the pure motion control of PVTOL (Hauser et al., 1992; Martin et al., 1996), is crucial for the aerial tool operation, where the quadrotor can experience sudden (escape-triggering) surges of its velocity after impacts with environments/objects (see Fig. 13); and (3) considered a different problem (i.e., pure motion control of PVTOL) with a focus on a different mechanism of non-minimum phase dynamics (i.e., "small force" due to slant wing-tip jets) and only the position tracking control by using a specific flat output (i.e., Huygens center of oscillation). Due to this reason, our results in this paper may be thought of as an extension (or re-finding) of Hauser et al. (1992) and Martin et al. (1996) to the quadrotor aerial tool operation with a complete analysis of its spatial/nonlinear (internal) dynamics and a novel control action to subdue its finite-time escape.

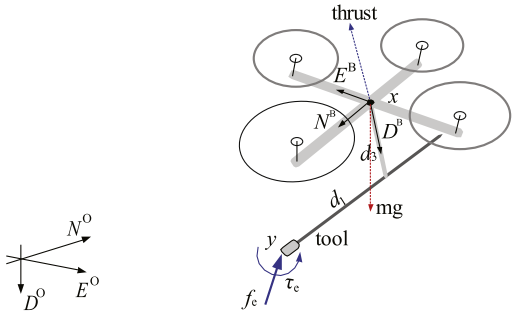

Fig. 1. Quadrotor-tool system: $\{O\} := \{N^o, E^o, D^o\}$ and $\{B\} := \{N^B, E^B, D^B\}$ are inertial and body frames, with thrust and gravity along D^B and D^o directions. Tool is attached at $d = [d_1, d_2, d_3] \in \Re^3$ expressed in $\{B\}$ with $d_2 = 0$.

Portions of this paper were presented in Lee and Ha (2012) and Nguyen and Lee (2013). The current manuscript integrates, refines and completes these results (Lee & Ha, 2012; Nguyen & Lee, 2013) under the unifying theme of quadrotor tool operation, with new derivation of the internal dynamics, new simulation results, and significantly improved readability. The current manuscript also features a newly-designed finite-time escape prevention control of Nguyen and Lee (2013) and a complete proof of its effectiveness, presented here for the first time.

The rest of the paper is organized as follows. The dynamics of quadrotor-tool system is derived and the condition to generate Cartesian control at its tool-tip is established in Section 2. The internal dynamics of spatial quadrotor tool operation is fully characterized in Section 3, with the seemingly counter-intuitive necessary condition for its stability revealed (i.e., tool above the quadrotor) and the finite-time escape prevention action designed/analyzed therein as well. The obtained theoretical results are then applied in Section 4 to the problems of rotating tool operation (i.e., screw-driver, vertical-jack) and hybrid position/force control against a working surface. Section 5 summarizes the paper with comments on future research.

2. Modeling and control generation of quadrotor-tool system

2.1. Dynamics modeling of quadrotor-tool system

Consider the quadrotor with a rigid tool as shown in Fig. 1. Similar to Brescianini et al. (2013) and Hehn and D'Andrea (2011), we assume that the tool is light enough (or counter-balanced with symmetric design) so that the center-of-mass of the total quadrotor-tool system is still close to that of the quadrotor. This assumption is adopted here only for simplicity: the results of this paper can be similarly derived when these two centers-of-mass are not coincident with each other.

With this assumption, the dynamics of the quadrotor-tool system can still be described by the well-known quadrotor

dynamics:

$$m\ddot{x} = -\lambda Re_3 + mge_3 + f_e \tag{1}$$

$$J\dot{\omega} + \omega \times J\omega = \tau + \tau_c, \qquad \dot{R} = RS(\omega) \tag{2}$$

where $x \in \Re^3$ is the quadrotor's center-of-mass position represented in the inertial frame $\{O\} := \{N^o, E^o, D^o\}$, $m > 0$ is the mass, $\lambda \in \Re$ is the thrust force, $R \in SO(3)$ represents the rotation of the body-frame $\{B\} := \{N^B, E^B, D^B\}$ w.r.t. $\{O\}$, $f_e \in \Re^3$ is the tool interaction force represented in $\{O\}$, g is the gravitation constant, and $e_3 = [0, 0, 1]^T$ is the basis vector specifying the down direction. Also, for (2), $J \in \Re^3$ is the body-fixed rotational inertia, $\omega := [\omega_1, \omega_2, \omega_3]^T \in \Re^3$ is the angular velocity of $\{B\}$ relative to $\{O\}$ represented in $\{B\}$, $\tau, \tau_c \in \Re^3$ are respectively the torque input and the external torque acting at the quadrotor's center-of-mass (defined below) all represented in $\{B\}$, and $S(\omega)\nu := \omega \times \nu$ for any $\nu \in \Re^3$.

Now, as in Fig. 1, denote by $d = [d_1, d_2, d_3]^T \in \Re^3$ the tool-tip position y from the quadrotor's center-of-mass x expressed in $\{B\}$. Then, the tool-tip position y in the inertial frame $\{O\}$ can be written as

$$y = x + Rd. \tag{3}$$

For simplicity, in this paper, we assume $d_2 = 0$. We also assume the tool is interacting with the environment only through its tool-tip y via the contact force $f_e \in \Re^3$ and the moment $\tau_e \in \Re^3$, with other external effects (e.g., aerodynamics force) much less than them. Then, τ_c in (2) is given by $\tau_c = d \times R^T f_e + R^T \tau_e$, with $R^T f_e$ and $R^T \tau_e$ being f_e and τ_e represented in $\{B\}$.

2.2. Cartesian control generation at the tool-tip y

In contrast to the motion control of quadrotor center-of-mass x, for the quadrotor tool operation, as can be seen from (3), we need to control both the translation x and the rotation R of the quadrotor at the same time. To better see this, we first transform the dynamics (1) into that of the tool-tip position y. For this, differentiating (3), we can obtain

$$\dot{y} = \dot{x} + RS(\omega)d, \qquad \ddot{y} = \ddot{x} + R[S(\dot{\omega}) + S^2(\omega)]d$$

and, injecting these relations to (1), we can achieve the dynamics of the tool-tip position y s.t.,

$$m\ddot{y} = u + f_e \tag{4}$$

where

$$u := mR[S(\dot{\omega}) + S^2(\omega)]d - \lambda Re_3 + mge_3 \in \Re^3 \tag{5}$$

is the Cartesian control action at the tool-tip position y, which is generated by $\lambda \in \Re$ and $\dot{w} \in \Re^3$.

The dynamics (4) with (5) now clearly shows that the tool control u requires simultaneous control of the quadrotor's translation (i.e., λ) and rotation (i.e., $\dot{\omega}$). An immediate question would then be whether it is possible to generate *any* desired control $u \in \Re^3$ via some combination of $(\lambda, \dot{\omega})$, and, if so, how. Here, we consider $\dot{\omega}$ as the control input with the assumption that τ in (2) is strong enough, since, in this case, we can directly assign any value $\dot{\omega}^d \in \Re^3$ to $\dot{\omega}$ via the control torque τ in (2) (e.g., via (7)). With $\dot{\omega}$ and λ as the control inputs, we can rewrite (5) s.t.,

$$\begin{bmatrix} 0 & -d_3 & d_2 \\ d_3 & 0 & -d_1 \\ -d_2 & d_1 & 0 \end{bmatrix} \begin{pmatrix} \dot{\omega}_1 \\ \dot{\omega}_2 \\ \dot{\omega}_3 \end{pmatrix} + \frac{1}{m} \begin{pmatrix} 0 \\ 0 \\ \lambda \end{pmatrix}$$

$$= S^2(\omega)d + gR^T e_3 - \frac{1}{m} R^T u \tag{6}$$

where we use $S(\dot{\omega})d = -S(d)\dot{\omega}$ and $u \in \Re^3$ is the desired Cartesian control at the tool-tip position y (4). The following Theorem 1 is a direct consequence of the structure of this control generation equation (6).

Theorem 1. *Given $(\lambda, \dot{\omega}_1, \dot{\omega}_2, \dot{\omega}_3)$ as the control input, the left hand side (LHS) of (6) can produce any desired Cartesian control $u \in \Re^3$ if and only if $d_3 \neq 0$.*

Proof. For sufficiency, note that, if $d_3 \neq 0$, we can generate any value u for the first and second lines in the LHS of (6) by using $\dot{\omega}_2, \dot{\omega}_3$, while that for the last line by using λ. For necessity, suppose $d_3 = 0$. Then, the first and second lines of the LHS are generated only by $\dot{\omega}_3$ (even if $d_2 \neq 0$), implying that the LHS of (6) cannot produce arbitrary control action u. ■

This Theorem 1 implies that, to achieve a desired control $u \in \Re^3$ for the y-dynamics, we must have $d_3 \neq 0$, i.e., the tool-tip position y, when expressed in $\{B\}$, needs to be strictly above, or strictly below, the quadrotor's center-of-mass x. This Theorem 1 is valid even if $d_2 \neq 0$.

If $d_3 \neq 0$, we can then utilize (6) to compute the thrust command λ and angular acceleration command $\dot{\omega}_1^d$, $\dot{\omega}_2^d$ for any given desired tool-tip Cartesian control $u \in \Re^3$. The remaining command $\dot{\omega}_3^d$ is redundant and can be simply set to be zero or utilized for other purpose (e.g., see Section 3.3). To achieve $\dot{\omega} \to \dot{\omega}^d$, we may then use the following simple PI-control with feedforward cancellation:

$$\tau = \omega \times J\omega + J\left(\dot{\omega}^d - k\left[\omega - \int_0^t \dot{\omega}^d(s)ds\right]\right) - \tau_c \tag{7}$$

where $k > 0$ is the I-control gain. The closed-loop attitude dynamics is then given by $\dot{e}_\omega + ke_\omega = 0$, with $e_\omega := \omega(t) - \int_0^t \dot{\omega}^d(s)ds$, implying $\dot{\omega} \to \dot{\omega}^d$, as long as τ is powerful enough as assumed so above. Since the attitude dynamics (2) is fully-actuated and passive, many control techniques can also be used here even in the presence of uncertainty or absence of force sensing (e.g., sliding mode control Slotine & Li, 1991 and Spong, Hutchinson, & Vidyasaga, 2006).

It may then appear that, as long as $d_3 \neq 0$, we can generate any arbitrary control u and drive the y-dynamics (3) however we want. This, however, may not be possible, since the control generation equation (6) defines a dynamic relation among $\dot{w}(\approx \dot{w}^d)$, w and R, which may be unstable. As shown in Section 3.1, this dynamics, unobservable from the y-dynamics, in fact constitutes the internal dynamics (Sepulchre et al., 1997; Slotine & Li, 1991) of the quadrotor tool operation, which arises because the tool-tip y control requires both the translation and attitude control, yet, the quadrotor is under-actuated only with the four actuations $(\lambda, \tau) \in \Re^4$. In the next Section 3, we analyze this internal dynamics of quadrotor tool operation, reveal a (seemingly counter-intuitive) structural condition to avoid internal instability, show that this internal dynamics can exhibit finite-time escape, and propose a stabilizing control to prevent that.

3. Internal dynamics and stability of quadrotor tool operation

3.1. Internal dynamics

Although Eq. (6) contains three rows, all of them may not constitute the internal dynamics, since: (1) the arbitrarily-assignable thrust input λ may effectively eliminate one-dimension of the internal dynamics (6); and (2) $\text{rank}[S(d)] = 2$, thus, only two-dimensional vector space among all possible $\dot{w}^d \in \Re^3$ are relevant to the internal dynamics. To overcome this geometric complication, instead of ω, we utilize the transformed angular velocity $\nu := [\nu_1, \nu_2, \nu_3]^T \in \Re^3$ as defined by

$$\omega = \frac{1}{\bar{d}} \begin{bmatrix} -d_3 & 0 & d_1 \\ 0 & \bar{d} & 0 \\ d_1 & 0 & d_3 \end{bmatrix} \nu =: \Sigma\nu \tag{8}$$

where $\bar{d} =: \sqrt{d_1^2 + d_3^2}$ and $\Sigma = \Sigma^T = \Sigma^{-1}$. See Fig. 2 for an illustration of ν and ω. Here, with $d_2 = 0$ as assumed above, the last column of Σ characterizes the nullspace of $S(d)$, while the first two the row space of $S(d)$. Different velocity space decompositions were also used in Hehn and D'Andrea (2011, virtual body frame) and Lee and Li (2013, passive decomposition) to facilitate dynamics analysis and control design.

Using the transformed angular velocity ν of (8), we can rewrite (6) s.t.,

$$\begin{pmatrix} -d_3\dot{\nu}_2 \\ -\bar{d}\dot{\nu}_1 \\ d_1\dot{\nu}_2 \end{pmatrix} + \begin{pmatrix} d_1\nu_1^2 + d_1\nu_2^2 + d_3\nu_1\nu_3 \\ -\bar{d}\nu_2\nu_3 \\ d_3\nu_1^2 + d_3\nu_2^2 - d_1\nu_1\nu_3 \end{pmatrix} + \frac{1}{m}\begin{pmatrix} 0 \\ 0 \\ \lambda \end{pmatrix} = gR^Te_3 - \frac{1}{m}R^Tu \tag{9}$$

where the first two rows define the internal dynamics of $\dot{\nu}_1$ and $\dot{\nu}_2$, yet, the third row that of none, since we can arbitrarily assign λ to match the third row of RHS without creating any internal dynamics. Note also that there is no internal dynamics of $\dot{\nu}_3$. This $\dot{\nu}_3$ in fact vanishes when (8) is combined with (6), which can also be seen from Fig. 2 that $\dot{\nu}_3$ induces no motion at the tool-tip y.

The internal dynamics in (9), yet, is rather difficult to analyze, since the quadrotor's rotation is expressed by the non-vector quantity $R \in \mathrm{SO}(3)$. To render (9) more amenable to analysis, here, we parameterize R using the yaw, pitch and roll angles, $(\phi, \theta, \psi) =: q \in \Re^3$, that is,

$$R = \begin{bmatrix} \mathrm{c}\phi\mathrm{c}\theta & -\mathrm{s}\phi\mathrm{c}\psi + \mathrm{c}\phi\mathrm{s}\theta\mathrm{s}\psi & \mathrm{s}\phi\mathrm{s}\psi + \mathrm{c}\phi\mathrm{s}\theta\mathrm{c}\psi \\ \mathrm{s}\phi\mathrm{c}\theta & \mathrm{c}\phi\mathrm{c}\psi + \mathrm{s}\phi\mathrm{s}\theta\mathrm{s}\psi & -\mathrm{c}\phi\mathrm{s}\psi + \mathrm{s}\phi\mathrm{s}\theta\mathrm{c}\psi \\ -\mathrm{s}\theta & \mathrm{c}\theta\mathrm{s}\psi & \mathrm{c}\theta\mathrm{c}\psi \end{bmatrix}$$

with $|\theta| < \pi/2$ and $\mathrm{s}\star = \sin\star$, $\mathrm{c}\star = \cos\star$ (Spong et al., 2006). We then have the following kinematic relation:

$$\begin{pmatrix} \dot{\phi} \\ \dot{\theta} \\ \dot{\psi} \end{pmatrix} = \Gamma\omega = \Gamma\Sigma\nu, \qquad \Gamma(\theta, \psi) := \frac{1}{\mathrm{c}\theta}\begin{bmatrix} 0 & \mathrm{s}\psi & \mathrm{c}\psi \\ 0 & \mathrm{c}\theta\mathrm{c}\psi & -\mathrm{c}\theta\mathrm{s}\psi \\ \mathrm{c}\theta & \mathrm{s}\theta\mathrm{s}\psi & \mathrm{s}\theta\mathrm{c}\psi \end{bmatrix} \tag{10}$$

and, combining (9) and (10) with the fact that gR^Te_3 is a function of only (θ, ψ), we can obtain the following four-dimensional dynamics:

$$\frac{d}{dt}\begin{pmatrix} \theta \\ \psi \\ \nu_1 \\ \nu_2 \end{pmatrix} = \mathcal{F}(\theta, \psi, \nu_1, \nu_2) + \begin{pmatrix} -\frac{d_3\mathrm{s}\psi}{\bar{d}}\nu_3 \\ \frac{d_1 + d_3\mathrm{t}\theta\mathrm{c}\psi}{\bar{d}}\nu_3 \\ \frac{1}{\bar{d}}u_2' - \nu_2\nu_3 \\ \frac{1}{d_3}u_1' + \nu_1\nu_3 \end{pmatrix} \tag{11}$$

where the drift vector field $\mathcal{F}(\theta, \psi, \nu_1, \nu_2)$ is given by

$$\mathcal{F}(\theta, \psi, \nu_1, \nu_2) = \begin{pmatrix} -\frac{d_1}{\bar{d}}\nu_1\mathrm{s}\psi + \nu_2\mathrm{c}\psi \\ -\frac{d_3}{\bar{d}}\nu_1 + \frac{d_1}{\bar{d}}\nu_1\mathrm{t}\theta\mathrm{c}\psi + \nu_2\mathrm{t}\theta\mathrm{s}\psi \\ -\frac{g}{\bar{d}}\mathrm{c}\theta\mathrm{s}\psi \\ -\gamma(\nu_1^2 + \nu_2^2) + \frac{g}{d_3}\mathrm{s}\theta \end{pmatrix} \in \Re^4$$

with $\gamma := -\frac{d_1}{d_3}$, $u' = [u_1', u_2', u_3']^T := \frac{1}{m}R^Tu$, and $\mathrm{t}\star := \tan\star$.

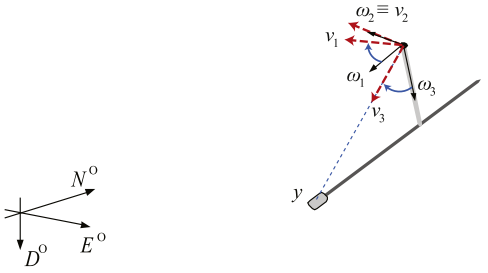

Fig. 2. Illustration of angular velocity $\omega = [\omega_1, \omega_2, \omega_3]^T$ and the transformed angular velocity $\nu = [\nu_1, \nu_2, \nu_3]^T$.

This four-dimensional dynamics (11) completely describes the internal dynamics of the quadrotor tool operation, which arises due to the quadrotor's under-actuation. In fact, this four-dimensional dynamics (11) is the internal dynamics (Slotine & Li, 1991), if we choose the output $(y, \phi) \in \Re^4$ and the state $(y, \dot{y}, q, \nu) \in \Re^{12}$ with the input $(\lambda, \tau) \in \Re^4$. More precisely, (1) each of these output variables has relative degree two, thus, the internal dynamics should be of four-dimension as (11); (2) the internal dynamics (11), which specifies the "internal" quadrotor rotation necessary to drive the tool-tip position y, can be obtained by twice-differentiating y with (10); and (3) the yaw angle ϕ has relative degree two with $\dot{\nu}_3$ as the input, which unlike $\dot{\nu}_2$, $\dot{\nu}_3$ in (11), is not required for the control generation equation (9), thus, any value can be assigned to $\dot{\nu}_3$ without affecting the internal dynamics and also the generation of the control u for the y-dynamics (4).

3.2. Structural condition of zero dynamics instability

In this Section 3.2, we analyze stability property of the internal dynamics (11) around its equilibriums and elucidate a seemingly counter-intuitive structural condition for its stability, i.e., the tool-tip y should be installed above the quadrotor's center-of-mass x, not below it. For this, we first define the zero dynamics by constraining (11) to the zero output manifold (i.e., $(y, \phi) \equiv 0$). More specifically, we obtain the following conditions for the internal dynamics (11): $\ddot{u}_1' = \ddot{u}_2' = 0$ from $\ddot{y} = 0$ in (4); and

$$d_3\nu_3 = -d_1\nu_1 - \bar{d}\nu_2\tan\psi$$

from $\dot{\phi} = 0$ in (10). Applying these conditions to (11), we can achieve the zero dynamics as follows:

$$\frac{d}{dt}\begin{pmatrix} \theta \\ \psi \\ \nu_1 \\ \nu_2 \end{pmatrix} = \begin{pmatrix} \frac{1}{\mathrm{c}\psi}\nu_2 \\ -\frac{\bar{d}}{d_3}\nu_1 + \gamma\nu_2\mathrm{t}\psi \\ -\frac{g}{\bar{d}}\mathrm{c}\theta\mathrm{s}\psi - \gamma\nu_1\nu_2 + \frac{\bar{d}}{d_3}\nu_2^2\mathrm{t}\psi \\ \frac{g}{d_3}\mathrm{s}\theta - \frac{\bar{d}}{d_3}\mathrm{t}\psi\nu_1\nu_2 - \gamma\nu_2^2 \end{pmatrix}. \tag{12}$$

From (12), we can show the zero-dynamics possesses the two equilibriums: $[\theta, \psi, \nu_1, \nu_2] = [0, 0, 0, 0]$ and $[\theta, \psi, \nu_1, \nu_2] = [0, \pi, 0, 0]$, with the former representing the quadrotor upright hovering posture, while the latter the upside-down hovering posture. See Fig. 3. We linearize the zero-dynamics (12) around these two equilibriums. First, around the equilibrium $[\theta, \psi, \nu_1, \nu_2] = [0, 0, 0, 0]$, we can obtain:

$$\begin{pmatrix} \dot{\theta} \\ \dot{\psi} \\ \dot{\nu}_1 \\ \dot{\nu}_2 \end{pmatrix} = \begin{bmatrix} 0 & 0 & 0 & 1 \\ 0 & 0 & -\frac{\bar{d}}{d_3} & 0 \\ 0 & -\frac{g}{\bar{d}} & 0 & 0 \\ \frac{g}{d_3} & 0 & 0 & 0 \end{bmatrix}\begin{pmatrix} \theta \\ \psi \\ \nu_1 \\ \nu_2 \end{pmatrix} \tag{13}$$

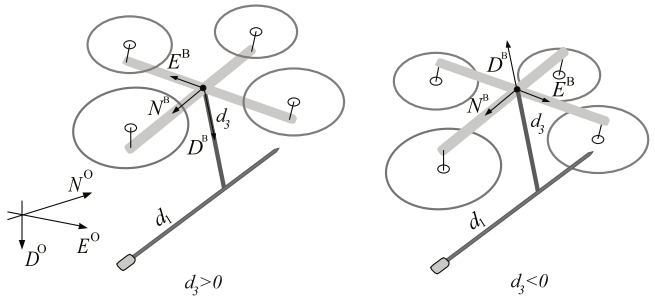

Fig. 3. Unstable configuration of zero-dynamics: $(\theta, \psi, \nu_1, \nu_2) = (0, 0, 0, 0)$ with $d_3 > 0$ (left); and $(\theta, \psi, \nu_1, \nu_2) = (0, \pi, 0, 0)$ with $d_3 < 0$ (right).

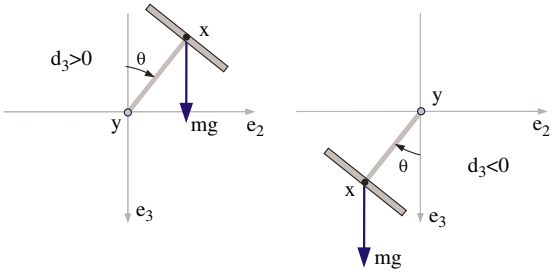

Fig. 4. Effect of d_3 on internal dynamics: (1) if $d_3 > 0$, gravity serves positive-feedback similar to inverted pendulum; (2) if $d_3 < 0$, negative-feedback similar to downward pendulum.

with the characteristic polynomial given by $\lambda^4 - 2\frac{g}{d_3}\lambda^2 + \frac{g^2}{d_3^2} = 0$ and the four eigenvalues given by $\lambda^2 = \frac{g}{d_3}$, implying that, if $d_3 > 0$, the zero-dynamics is unstable around the equilibrium $[\theta, \psi, \nu_1, \nu_2] = [0, 0, 0, 0]$.

On the other hand, for the equilibrium $[\theta, \psi, \nu_1, \nu_2] = [0, \pi, 0, 0]$, the linearization of the zero-dynamics (12) yields

$$\begin{pmatrix} \dot\theta \\ \dot\psi \\ \dot\nu_1 \\ \dot\nu_2 \end{pmatrix} = \begin{bmatrix} 0 & 0 & 0 & -1 \\ 0 & 0 & -\frac{\bar d}{d_3} & 0 \\ 0 & \frac{g}{\bar d} & 0 & 0 \\ \frac{g}{d_3} & 0 & 0 & 0 \end{bmatrix} \begin{pmatrix} \theta \\ \psi \\ \nu_1 \\ \nu_2 \end{pmatrix} \tag{14}$$

with the characteristic polynomial given by $\lambda^4 + 2\frac{g}{d_3}\lambda^2 + \frac{g^2}{d_3^2} = 0$ and the four eigenvalues given by $\lambda^2 = -\frac{g}{d_3}$, implying that, if $d_3 < 0$, the zero-dynamics (11) will be unstable around the equilibrium $[\theta, \psi, \nu_1, \nu_2] = [0, \pi, 0, 0]$. Note that these two unstable equilibriums of the zero-dynamics, $(\theta, \psi, \nu_1, \nu_2) = (0, 0, 0, 0)$ with $d_3 > 0$ for (13) and $(\theta, \psi, \nu_1, \nu_2) = (0, \pi, 0, 0)$ with $d_3 < 0$ for (14), represent the same configuration, that is, the quadrotor hovers with the tool-tip y located below the quadrotor's center-of-mass x. See Fig. 3.

This observation then shows that, for internal stability of the quadrotor tool operation, the tool-tip y should be located *above* the quadrotor's center-of-mass x, not below it, even though the latter would appear more reasonable at a first glance and also typically aimed for in practice. The above analysis also shows that, if y is located above x, the internal dynamics may be stable, which we indeed observed from our simulation with some viscous damping effect (e.g., aerodynamics dissipation), when the quadrotor angular velocity ω is not so fast and $|\gamma| = |d_1/d_3|$ is not so large. This seemingly counter-intuitive necessary condition for the internal dynamics stability is summarized in the following Theorem 2.

Theorem 2. *Consider the quadrotor tool operation system (1)–(2) with a rigid/light tool attached with its tool-tip y located at $d = [d_1, 0, d_3]^T$ as measured in $\{B\}$ from the quadrotor center-of-mass x. Then, a necessary condition to avoid internal dynamics instability is $d_3 < 0$ for the equilibrium $(\theta, \psi, \nu_1, \nu_2) = (0, 0, 0, 0)$ or $d_3 > 0$ for the equilibrium $(\theta, \psi, \nu_1, \nu_2) = (0, \pi, 0, 0)$, both implying the tool-tip y should be above the center-of-mass x, not below it.*

This Theorem 2 can also be understood as follow. If the tool-tip y is located below the quadrotor's center-of-mass x (e.g., $d_3 > 0$ for upright hovering posture) and if we want, for example, to regulate the tool-tip position, the thrust and angular torque inputs will be used up to maintain this tool-tip position, yet, the gravity will still pull the system down similar to the case of an inverted pendulum—see Fig. 4. This similarity is also evident in (13), where the zero dynamics has a saddle equilibrium with two unstable and two stable poles (i.e., (13) at $(\theta, \psi, \nu_1, \nu_2) = (0, 0, 0, 0)$ with $d_3 > 0$). On the other hand, if the tool-tip y is above x (e.g., $d_3 < 0$ for upright hovering posture), the system would behave similar to the stable downward pendulum as again can be seen from (13) with pure imaginary poles when $d_3 < 0$ (right plot of Fig. 4). Note also that Theorem 2 holds regardless of any ν_3-action (16).

Even if we upheld the necessary condition of Theorem 2, sometimes, we could still observe (fairly severe) instability of the internal dynamics, particularly when the quadrotor's angular velocity ω gets faster with a large $|\gamma| = |d_1/d_3|$. This is in fact due to the quadratic terms (i.e., $\gamma(\nu_1^2 + \nu_2^2)$) in (11), which can trigger finite-time escape (Sepulchre et al., 1997). In the next Section 3.3, we analyze this finite-time escape and propose a stabilizing control action to prevent that.

3.3. Finite-time escape prevention

To facilitate analysis of finite-time escape and synthesis of the control action to prevent that, we rewrite the dynamics of ν_1 and ν_2 in (11) s.t.,

$$\begin{pmatrix} \dot\nu_1 \\ \dot\nu_2 \end{pmatrix} = \begin{pmatrix} 0 \\ -\gamma(\nu_1^2 + \nu_2^2) \end{pmatrix} + \begin{bmatrix} 0 & -\nu_3 \\ \nu_3 & 0 \end{bmatrix} \begin{pmatrix} \nu_1 \\ \nu_2 \end{pmatrix} + \begin{pmatrix} \bar u_1 \\ \bar u_2 \end{pmatrix} \tag{15}$$

where $\gamma = -\frac{d_1}{d_3}$, $\bar u_1 := \frac{-gc\theta s\psi + u_2'}{\bar d}$ and $\bar u_2 := \frac{gs\theta + u_1'}{d_3}$. Here, without loss of generality, we assume $d_1 > 0$. We also choose $d_3 < 0$ to respect the necessary condition for internal stability of Theorem 2. We then have $\gamma > 0$. We can then see from (15) that the quadratic terms with γ in (15) will always pull (ν_1, ν_2) downward in the (ν_1, ν_2)-plane (see Fig. 5) and, moreover, can induce finite-time escape when $\nu_2 < 0$. We can see from (15) that this tendency would be more intense with larger $|\gamma| = |d_1/d_3|$ and faster (ν_1, ν_2). We may also consider $\bar u_1, \bar u_2$ in (15) as bounded disturbance, as the desired control u is bounded (with $u' = (1/m)R^T u$).

To prevent the finite-time escape, here, we attempt to utilize ν_3 to regulate (ν_1, ν_2). Recall from Section 3.1 that this ν_3 can be arbitrarily assigned without affecting the tool-tip control u generation (6). This ν_3-action, however, is limited, as its action is embedded in the skew-symmetric matrix in (15), thus, is only norm-preserving with its direction always tangential to the circle in the (ν_1, ν_2)-plane with the radius of $\sqrt{\nu_1^2 + \nu_2^2}$ and the center at the origin.

With this circumferential ν_3-action, we may still think of the following strategy. Since the quadratic terms with γ in (15) always pull down (ν_1, ν_2) along the ν_2-axis and can trigger the finite-time escape only when $\nu_2 < 0$, when ν_2 proceeds down along the ν_2-axis, if we can apply large enough ν_3-action to "swing up" (ν_1, ν_2) back to the upper-side of the (ν_1, ν_2)-plane (i.e., $\nu_2 \geq 0$) in a suitable way to ensure the boundedness of ν_1 as well, we would be able to prevent the finite-time escape even with only this limited ν_3-action.

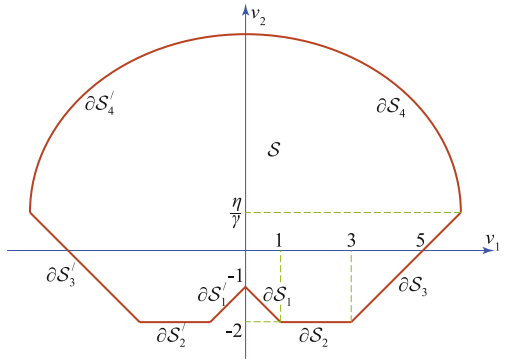

Fig. 5. Invariant set $\mathcal{S}$ with finite-time escape prevention.

To achieve this strategy, we design the ν_3-action s.t.,

$$\nu_3 := \gamma\nu_1(1+\nu_2^2) + \rho\,\mathrm{sgn}(\nu_1) \tag{16}$$

where $\rho := 2\eta - \gamma\nu_2$, with $\eta > 0$ defined s.t., $\eta > (|\bar{u}_1(t)| + |\bar{u}_2(t)|)/2\ \forall t \geq 0$, and $\mathrm{sgn}(\nu_1) = 1$ if $\nu_1 \geq 0$ and $\mathrm{sgn}(\nu_1) = -1$ if $\nu_1 < 0$.

Theorem 3. *Consider the dynamics (15) under the ν_3-action (16) with $\gamma \geq 0$. Then, there exists a positive-invariant compact set $\mathcal{S} \subset \left\{(\nu_1,\nu_2) \mid \nu_1^2+\nu_2^2 \leq \left(\frac{\eta}{\gamma}+5\right)^2 + \frac{\eta^2}{\gamma^2}\right\}$ s.t., if $(\nu_1(0),\nu_2(0)) \in \mathcal{S}$, $(\nu_1(t),\nu_2(t)) \in \mathcal{S}\ \forall t \geq 0$.*

Proof. Let us first define the compact set $\mathcal{S}$ with its boundary given by $\partial\mathcal{S} := \bigcup_i \partial\mathcal{S}_i + \bigcup_i \partial\mathcal{S}_i'$, where

$$\partial\mathcal{S}_1 := \{(\nu_1,\nu_2) \mid \nu_2 = -\nu_1 - 1, 0 \leq \nu_1 \leq 1\}$$
$$\partial\mathcal{S}_2 := \{(\nu_1,\nu_2) \mid \nu_2 = -2, 1 \leq \nu_1 \leq 3\}$$
$$\partial\mathcal{S}_3 := \left\{(\nu_1,\nu_2) \mid \nu_1 = \nu_2 + 5, -2 \leq \nu_2 \leq \tfrac{\eta}{\gamma}\right\}$$
$$\partial\mathcal{S}_4 := \left\{(\nu_1,\nu_2) \mid \nu_1^2+\nu_2^2 = \left(\tfrac{\eta}{\gamma}+5\right)^2 + \tfrac{\eta^2}{\gamma^2},\ \tfrac{\eta}{\gamma} \leq \nu_2 \leq \sqrt{\left(\tfrac{\eta}{\gamma}+5\right)^2 + \tfrac{\eta^2}{\gamma^2}}\right\}$$

and $\partial\mathcal{S}_i' := \{(-\nu_1,\nu_2) \mid (\nu_1,\nu_2) \in \partial\mathcal{S}_i\}$. See Fig. 5

To show that the set $\mathcal{S}$ is positive-invariant, here, we show that the vector field $(\dot{\nu}_1,\dot{\nu}_2)$ of (15) under the ν_3-action (16) always points inward $\mathcal{S}$ along its boundary $\partial\mathcal{S}$. For this, note that ν_3 in (16) is an odd function w.r.t. ν_1. This then implies that $\dot{\nu}_1$ and $\dot{\nu}_2$ in (15) are respectively odd and even functions w.r.t., ν_1. Therefore, if we can show that $(\dot{\nu}_1,\dot{\nu}_2)$ points inward $\mathcal{S}$ along the right half of $\partial\mathcal{S}$, the same will also be true for the other half $\partial\mathcal{S}'$. We now analyze the vector field $(\dot{\nu}_1,\dot{\nu}_2)$ along each segment $\partial\mathcal{S}_i$ of the right half of $\partial\mathcal{S}$.

• On the boundary $\partial\mathcal{S}_1$ (see Fig. 6(a)), we have

$$\begin{aligned}\dot{\nu}_1 &= -\gamma\nu_1\nu_2(1+\nu_2^2) - \rho\nu_2 + \bar{u}_1\\ &= \gamma\nu_1|\nu_2|(1+\nu_2^2) + \rho|\nu_2| + \bar{u}_1 > \rho|\nu_2| + \bar{u}_1 > 0\end{aligned}$$

with $\rho = \gamma|\nu_2| + 2\eta > |\bar{u}_1|$ and $|\nu_2| \geq 1$ on $\partial\mathcal{S}_1$. On the other hand, on $\partial\mathcal{S}_1$, $\dot{\nu}_2$ can be positive or negative. If $\dot{\nu}_2 \geq 0$, the vector $(\dot{\nu}_1,\dot{\nu}_2)$ will point inward $\mathcal{S}$, thus, here, we only consider the case $\dot{\nu}_2 < 0$, for which $(\dot{\nu}_1,\dot{\nu}_2)$ points inwards if

$$\dot{\nu}_1 \geq -\dot{\nu}_2 \tag{17}$$

or, using (15) with (16),

$$\gamma\nu_1|\nu_2|(1+\nu_2^2) + \rho|\nu_2| + \bar{u}_1 \geq -\gamma\nu_2^2(\nu_1^2-1) - \rho\nu_1 - \bar{u}_2.$$

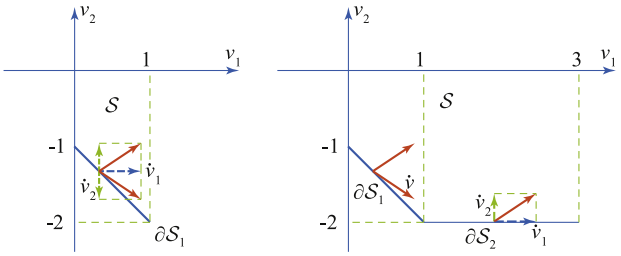

(a) $(\dot{\nu}_1,\dot{\nu}_2)$ on $\partial\mathcal{S}_1$. (b) $(\dot{\nu}_1,\dot{\nu}_2)$ on $\partial\mathcal{S}_2$.

Fig. 6. The vector field $(\dot{\nu}_1,\dot{\nu}_2)$ points inward the set $\mathcal{S}$ along the boundaries $\partial\mathcal{S}_1$ and $\partial\mathcal{S}_2$.

Since, on $\partial\mathcal{S}_1$, we have $\gamma\nu_1|\nu_2|(1+\nu_2^2) \geq 0$ and $-\gamma\nu_2^2\nu_1^2 - \rho\nu_1 \leq 0$, (17) will be satisfied if

$$\rho|\nu_2| + \bar{u}_1 \geq \gamma\nu_2^2 + |\bar{u}_2| \tag{18}$$

which is indeed true, since, substituting $\rho = 2\eta + \gamma|\nu_2|$ on $\partial\mathcal{S}_1$ into (18) yields

$$\gamma\nu_2^2 + 2\eta|\nu_2| + \bar{u}_1 \geq \gamma\nu_2^2 + |\bar{u}_2|$$

which holds, since, on $\partial\mathcal{S}_1$, $|\nu_2| \geq 1$, thus, $2\eta|\nu_2| > |\bar{u}_1| + |\bar{u}_2|$. This shows that, on segment $\partial\mathcal{S}_1$, the vector field $(\dot{\nu}_1,\dot{\nu}_2)$ points inwards the set $\mathcal{S}$, as depicted in Fig. 6(a).

• On the boundary $\partial\mathcal{S}_2$ (see Fig. 6(b)), from (15) with (16), we have

$$\dot{\nu}_1 > \rho|\nu_2| + \bar{u}_1 = 2\eta|\nu_2| + \gamma|\nu_2|^2 + \bar{u}_1 > 0$$
$$\dot{\nu}_2 \geq \rho\nu_1 + \bar{u}_2 = (2\eta + \gamma|\nu_2|)|\nu_1| + \bar{u}_2 > 0$$

since $\nu_1 \geq 1$, $\nu_2 = -2$ and $\rho = 2\eta + \gamma|\nu_2| > |\bar{u}_1| + |\bar{u}_2|$ on $\partial\mathcal{S}_2$, implying that the vector $(\dot{\nu}_1,\dot{\nu}_2)$ on the boundary $\partial\mathcal{S}_2$ also points into $\mathcal{S}$, as illustrated in Fig. 6(b).

• On the boundary $\partial\mathcal{S}_3$ (see Fig. 7), we have:

$$\rho = 2\eta - \gamma\nu_2 \geq \eta \tag{19}$$

with $-2 \leq \nu_2 \leq \eta/\gamma$. Then, similar to the case of $\partial\mathcal{S}_2$ above, we can show that

$$\dot{\nu}_2 > \rho\nu_1 + \bar{u}_2 > 0$$

since $\nu_1 \geq 3$ on $\partial\mathcal{S}_3$. On the other hand, along the boundary $\partial\mathcal{S}_3$, $\dot{\nu}_1$ can be positive or negative. If $\dot{\nu}_1$ is negative then the vector field points inwards. Thus, here, we only need to consider the case of $\dot{\nu}_1 \geq 0$.

When $\dot{\nu}_1 \geq 0$, the vector $(\dot{\nu}_1,\dot{\nu}_2)$ will point into $\mathcal{S}$ if

$$\dot{\nu}_2 \geq \dot{\nu}_1 \tag{20}$$

or, using (15) with (16) and (19), we can rewrite (20) s.t., $\gamma\nu_2^2(\nu_1^2-1) - \gamma\nu_1\nu_2 + 2\eta\nu_1 + \bar{u}_2 \geq -\gamma\nu_1\nu_2(1+\nu_2^2) + \gamma\nu_2^2 - 2\eta\nu_2 + \bar{u}_1$, which can be rearranged as

$$\gamma\nu_2^2(\nu_1^2-2) + 2\eta\nu_1 + \bar{u}_2 \geq -\gamma\nu_1\nu_2^3 - 2\eta\nu_2 + \bar{u}_1. \tag{21}$$

Now, for the boundary $\partial\mathcal{S}_3$, let us first consider the upper segment overlapped with the region $\{(\nu_1,\nu_2) \mid \nu_1 \geq 5, \nu_2 \geq 0\}$. Then, since $\gamma\nu_1\nu_2^3 + 2\eta\nu_2 \geq 0$ with $\nu_2 \geq 0$ and $\nu_1 > 0$, (21) will be attained if

$$\gamma\nu_2^2(\nu_1^2-2) + 2\eta\nu_1 + \bar{u}_2 \geq \bar{u}_1$$

which is satisfied, since $\nu_1 \geq 5$ on this segment. On the other hand, for the lower segment of $\partial\mathcal{S}_3$ within the region $\{(\nu_1,\nu_2) \mid 3 \leq \nu_1 < 5, -2 \leq \nu_2 < 0\}$, we can rewrite (21) as

$$\gamma\nu_2^2(\nu_1^2 - |\nu_2|\nu_1 - 2) + 2\eta(\nu_1 - |\nu_2|) + \bar{u}_2 \geq \bar{u}_1$$

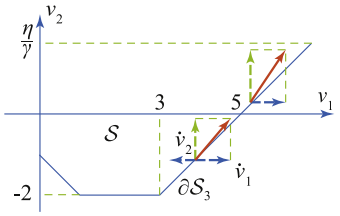

Fig. 7. The vector field $(\dot{\nu}_1, \dot{\nu}_2)$ along the boundary $\partial\mathcal{S}_3$.

which is also satisfied, since on this segment, $\nu_1^2 - |\nu_2|\nu_1 - 2 \geq 1$ and $\nu_1 - |\nu_2| \geq 1$. Thus proves that, on the boundary $\partial\mathcal{S}_3$, the vector $(\dot{\nu}_1, \dot{\nu}_2)$ points into the set $\mathcal{S}$.

• For the arc segment $\partial\mathcal{S}_4$, let us define

$$V := \frac{1}{2}(\nu_1^2 + \nu_2^2)$$

which then assumes a constant value along this segment, that is, $V(\nu_1, \nu_2) = \frac{1}{2}[(\eta/\gamma + 5)^2 + (\eta/\gamma)^2] > 25/2, \forall(\nu_1, \nu_2) \in \partial\mathcal{S}_4$. Differentiating this V with (15) with the fact that $\eta \geq \sqrt{\bar{u}_1^2 + \bar{u}_2^2}$, we can then obtain

$$\begin{aligned}\dot{V} &= -\gamma\nu_2(\nu_1^2 + \nu_2^2) + (\bar{u}_1\nu_1 + \bar{u}_2\nu_2) \\ &\leq -\eta(\nu_1^2 + \nu_2^2) + 2\eta\sqrt{\nu_1^2 + \nu_2^2} \leq -\eta(2V - 2\sqrt{2V}) < 0\end{aligned}$$

since, on $\partial\mathcal{S}_4$, $\nu_2 \geq \eta/\gamma$ and $\sqrt{V} > 5/\sqrt{2}$. This then implies that (ν_1, ν_2) evolves into the set $\mathcal{S}$ when it is on the boundary $\partial\mathcal{S}_4$—see Fig. 8. ■

This Theorem 3 shows that the ν_3-action (16), albeit limited as stated above, can indeed prevent the finite-time escape of the internal dynamics as long as $(\nu_1(0), \nu_2(0)) \in \mathcal{S}$. This also means that, using the ν_3-action (16) with $(\nu_1(0), \nu_2(0)) \in \mathcal{S}$ and also with the necessary condition of Theorem 2 satisfied, we can achieve any desired tool-tip position control $u \in \Re^3$ via (6) while avoiding the issue of internal dynamics instability. Mathematical proof of this finite-time escape is not available at the moment, although we indeed experienced many of its occurrences during our simulation study (e.g., see Fig. 13 and Lee & Ha, 2012, Fig. 3), which our ν_3-action turns out to be able to adequately subdue. A precise/mathematical treatment of this finite-time escape itself would require a significant technical development as in Getz and Jacobson (1977) and is beyond the scope of this paper.

The ν_3-action (16) contains the discontinuous function sgn(·), which poses an implementation problem since our control input is $(\lambda, \tau) \in \Re^4$. For this, we may replace sgn(ν_1) by its continuous approximation (e.g., sat(ν_1/ϵ) or $\frac{2}{\pi}$atan(ν_1/ϵ), with approximation layer $\epsilon > 0$). Note that this approximation would affect the ν_3-action (16) only around the two intersection points between the ν_2-axis and the boundary $\partial\mathcal{S}$ (see Fig. 5), implying that the resultant performance degradation would be only mild. In fact, we found, during our simulations (e.g., Section 4.2), that $\frac{2}{\pi}$atan(ν_1/ϵ) works just fine when used instead of sgn(ν_1). Note also that, if the task is formulated s.t., (ν_1, ν_2) is kept small enough (e.g., Section 4.1), the ν_3-action would not be necessary, since, in this case, the quadratic terms with γ in (15) will be dominated by other (e.g., linear) terms therein. The necessary condition of Theorem 2, yet, should still be enforced even in this case to avoid internal dynamics instability. See Section 4.1.

Our proposed ν_3-action (16) does not interfere at all with the generation of the tool-tip Cartesian control $u \in \Re^3$, since, as can be seen from (9), any desired control $u \in \Re^3$ can be generated only by using $(\dot{\nu}_1, \dot{\nu}_2, \lambda)$ regardless of ν_3. This ν_3-action, however, will produce some extra rotational motion of the quadrotor (e.g., $\dot{\phi}$ via (10)) on top of those necessary to generate the u-control through (9). This extra motion may then induce collision when the quadrotor is interacting with external environments/objects.

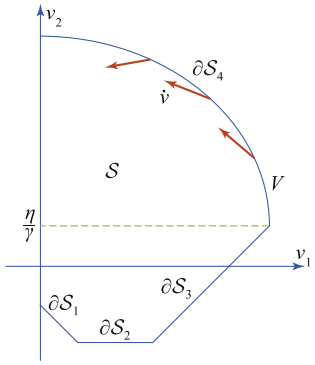

Fig. 8. The vector field $(\dot{\nu}_1, \dot{\nu}_2)$ along the boundary $\partial\mathcal{S}_4$.

One possible approach to avoid such collision, and further to endow the quadrotor-tool system with collision avoidance capability, is to activate the ν_3-action only when (ν_1, ν_2) is outside $\mathcal{S}$, while, when inside $\mathcal{S}$, exploit the ν_3-action for collision avoidance. This idea then naturally suggests to switch the ν_3-action (16) with $\partial\mathcal{S}$ as its switching surface. For this, the proposed ν_3-action (16) is not directly applicable, since, with (λ, τ) as the control input, we cannot instantaneously switch ν_3 on $\partial\mathcal{S}$. Instead, we would need to define a new switching surface $\partial\mathcal{S}_w \in \mathcal{S}$, whose gap from $\partial\mathcal{S}$ should be designed with the convergence rate of the ν_3-control and $(\dot{\nu}_1(t), \dot{\nu}_2(t))$ taken into account, so that, even with the (indirect) control τ, the ν_3-action is guaranteed to be activated before (ν_1, ν_2) escapes from $\mathcal{S}$, while also minimizing the gap between $\partial\mathcal{S}_w$ and $\partial\mathcal{S}$. How to design such switching ν_3-action with an optimal $\partial\mathcal{S}_w$ is a topic of future research.

4. Illustrative examples

In this Section 4, we apply our theoretical results to the two perhaps most practically-important aerial tool operation tasks, namely, (1) rotating tool operation, where the quadrotor itself serves as the actuator for some rotating tool (e.g., screw-driver, vertical-jack); and (2) hybrid force/position control, where the quadrotor controls its tool-tip y to follow some desired trajectory on a surface while exerting certain desired force normal to it.

4.1. Rotating tool operation

We consider two most representative rotating tool operations: (1) screw-driver operation (i.e., rotation about N^B-axis) and (2) vertical-jack operation (i.e., rotation about the E^B-axis). To operate these tools, the quadrotor should rotate itself while maintaining the contact at the tool-tip $y \in \Re^3$. This, however, is not possible for the quadrotor, since, being under-actuated, it cannot control the tool rotation ω and the tip position y at the same time.

To overcome this difficulty, here, we assume an external contact-keeping mechanism. One example of such mechanisms, assumed for the simulation here and also envisioned for our implementation, is a compliant coupling with magnetic-snapper. We then model the contact force $f_e \in \Re^3$ in (1) s.t., $f_e := -B\dot{y} - Ky$ with the contact point at $y = 0$. On the other hand, since τ is assumed to be strong enough, the quadrotor can generate any desired tool rotation while overcoming the contact torque τ_c in (2). We also do not implement the ν_3-action (16), as all the rotating tool

operations here (with $d_3 < 0$) are mild enough (with small enough ω), thus, do not trigger the finite-time escape. For the vertical-jack operation with $d_3 > 0$, we however indeed observed the finite-time escape phenomenon when the ν_3-action is deactivated—see (Lee & Ha, 2012) for more details on this.

Consider first the case of screw-driver operation. For simplicity, we assume this operation is along the N^B-axis from $R(0) = I$ while keeping $N^B \approx N^o$ and $y \approx 0$. The quadrotor's rotation matrix R is then given by

$$R(\psi) = \begin{bmatrix} 1 & 0 & 0 \\ 0 & \cos\psi & -\sin\psi \\ 0 & \sin\psi & \cos\psi \end{bmatrix}$$

with $\omega = [\dot{\psi}; 0; 0]$, where ψ is the roll angle. From (4)–(5), we can see that, if we incur this rotational motion ω, it will generate some contact force u, that may perturb the tool-tip contact. To avoid any tool-disengagement, we then attempt to minimize this perturbing force u (5), or, equivalently, to minimize the magnitude of

$$R^T u = \begin{pmatrix} 0 \\ -md_3\ddot{\psi} + mg\sin\psi \\ -md_3\dot{\psi}^2 - \lambda + mg\cos\psi \end{pmatrix} \tag{22}$$

so that it can still be absorbed by the contact-keeping mechanism (i.e., with small $\|f_e\|$).

This then suggests that, if we assign $\psi, \ddot{\psi}$ to satisfy the second line of (22) and λ to eliminate the third line of (22), we can achieve rotation while ensuring $R^T u = 0$ to maintain the tool-tip contact during the operation. Note here the similarity of the second line of (22) with the pendulum dynamics as observed in Section 3.2. This dynamics (22) is in fact the internal dynamics (11) constrained by $\dot{\phi} = \dot{\theta} = 0$. We then set $d_3 < 0$ according to Theorem 2 and define the desired roll angle $\psi_d(t)$ s.t.,

$$\psi_d(t) := \psi_{\max}\sin\omega_n t \tag{23}$$

with $\omega_n := \sqrt{\frac{g}{|d_3|}}$, which is the solution of the linearized dynamics of the second line of (22) about $\psi = 0$. We also choose the thrust command λ s.t.,

$$\lambda = mg\cos\psi - md_3\dot{\psi}^2$$

to eliminate the third line of (22), with the attitude torque τ defined similar to (7) s.t.,

$$\tau = \omega \times J\omega + J[\dot{\omega}_d - b(\omega - \omega_d) - k(q - q_d)] - \tau_c$$

with $\omega_d = [\dot{\psi}_d; 0; 0]$ and $q_d(t) = [\psi_d(t); 0; 0]$.

Simulation results of this screw-driver operation are presented in Fig. 9, where we can see that: (1) the quadrotor center-of-mass x makes a circular trajectory, evidencing the tool rotation (with the tool-tip y fixed); (2) both f_e and y are small, yet, not perfectly zero, since the trajectory ψ_d (23) is a solution of the linearized dynamics, not the original nonlinear dynamics in (22), and also we inject some parametric uncertainty when computing the control action (λ, τ); and (3) control actions $(\lambda, \tau_1, \tau_2)$ are relatively aggressive. To reduce this aggressiveness, we perform the same simulation with the rotation frequency slowed down to $\omega_n/2$. The results are overlaid in Fig. 9, where we can see that: (1) the control action becomes substantially smoother than before; (2) f_e and y become larger, as ψ_d, in this case, differs further from the solution of the original internal dynamics in (22); (3) the circular trajectory of x is also perturbed more due to the same reason; and (4) the tool-tip y is still maintained at $y = 0$ with contact-keeping mechanism strong enough.

Let us also consider the case of vertical-jack operation, which, for simplicity, we assume to occur about the axis of $E^B \approx E^o$ with $y \approx 0$. Then, similar to above, the rotation matrix R of the quadrotor is reduced to

$$R(\theta) = \begin{bmatrix} \cos\theta & 0 & \sin\theta \\ 0 & 1 & 0 \\ -\sin\theta & 0 & \cos\theta \end{bmatrix}$$

with $\omega = [0; \dot{\theta}; 0]$, where θ is the pitch angle, and the resultant contact force is given by

$$R^T u = \begin{pmatrix} md_3\ddot{\theta} - md_1\dot{\theta}^2 - mg\sin\theta \\ 0 \\ -md_1\ddot{\theta} - md_3\dot{\theta}^2 - \lambda + mg\cos\theta \end{pmatrix} \tag{24}$$

which we want to minimize to maintain tool-tip contact.

Similar to (22), the first line of (24) possesses the form of the pendulum dynamics as analyzed in Section 3.2. This dynamics (24) is the internal dynamics (11) constrained by $\dot{\phi} = \dot{\psi} = 0$. This internal dynamics (24) also shows that the vertical-jack operation is much more prone to the finite-time escape than the screwdriver operation. That is, the internal dynamics (24) contains quadratic term (e.g., $md_1\dot{\theta}^2$), which is able to trigger the finite-time escape as analyzed in Section 3.3 and is absent in the screwdriver operation internal dynamics (22).

We set $d_3 < 0$ according to Theorem 2 to avoid internal instability and choose the desired pitch profile $\theta_d(t)$ s.t.,

$$\theta_d(t) = \theta_{\max}\sin(\omega_n/2)t, \quad \omega_n = \sqrt{g/|d_3|} \tag{25}$$

where we adopt $\omega_n/2$ instead of ω_n, as the operation with ω_n exhibits finite-time escape (with the ν_3-action deactivated), whereas that with $\omega_n/2$ is mild enough not to induce its occurrence. With this slow-down $\omega_n/2$, of course, the perturbation force $R^T u$ becomes larger as it deviates further from the exact solution of (24). We apply the torque control τ as defined above to regulate $q = [\psi; \theta; \phi]$ to $q_d := [0; \theta_d(t); 0]$. To eliminate the third line of (24), we define the thrust input λ s.t.,

$$\lambda = -md_1\ddot{\theta}_d - md_3\dot{\theta}^2 + mg\cos\theta$$

where we use $\ddot{\theta}_d$ instead of $\ddot{\theta}$ as the latter is difficult to measure in practice, although this would produce more perturbation to the tool-tip contact.

Simulation results of this vertical-jack operation are presented in Fig. 10, where we can see that the quadrotor can stably perform the task. The contact force f_e becomes relatively large though, as we utilize $\omega_n/2$ instead of ω_n to avoid the finite-time escape. We also perform similar simulation with $d_3 > 0$ to intentionally violate the necessary condition of Theorem 2 and observe that the quadrotor is flipping over to converge to its stable equilibrium (i.e., tool above the quadrotor), yet, during this course, with the ν_3-action (16) deactivated, ω becomes large enough to trigger the finite-time escape (not shown here: see instead Lee & Ha, 2012, Fig. 3).

4.2. Hybrid position/force control

We first set $d_3 \neq 0$, so that, following Theorem 1, we can generate *any* Cartesian control action $u \in \Re^3$ at the tool-tip $y \in \Re^3$ by using (λ, τ) via (6), or, more precisely, by using $(\lambda, \dot{\nu}_1, \dot{\nu}_2)$ via (9). We may then consider the y-dynamics as a simple fully-actuated point mass dynamics (4), i.e.,

$$m\ddot{y} = u + f_e \tag{26}$$

where we can assign $u \in \Re^3$ arbitrarily and $f_e \in \Re^3$ is the interaction force between the tool-tip and the working surface. Once we have this fully-actuated y-dynamics (26), it becomes rather a standard task to design the hybrid position/force control for u.

Of course, this statement and the validity of (26) hinge upon the well-behavedness of the internal dynamics (11). To ensure

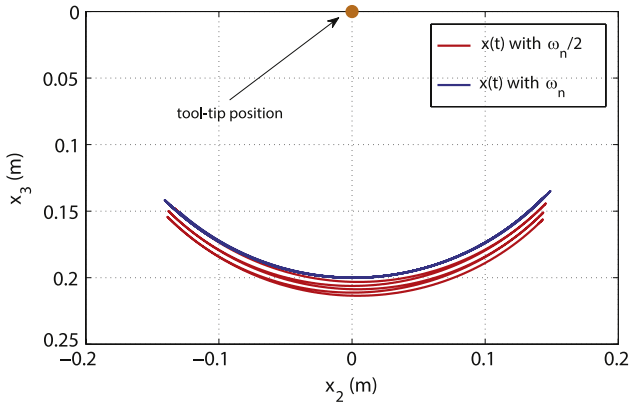

(a) Trajectory of quadrotor center-of-mass position x (positive x_3 implies downward direction).

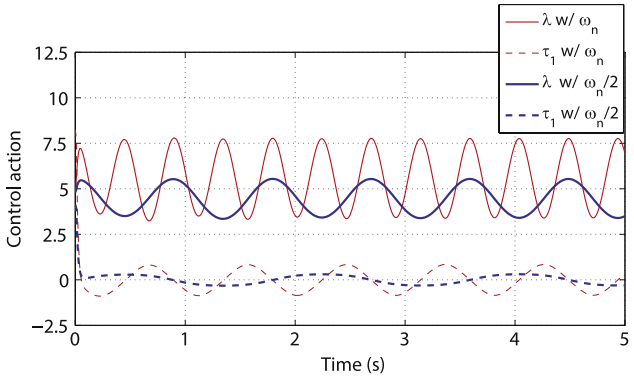

(b) Control action λ, τ.

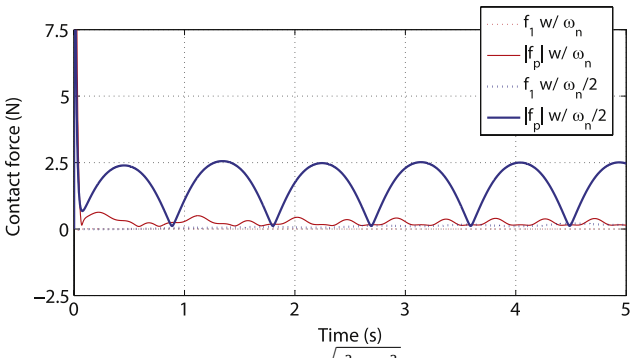

(c) Contact force f_e (with $f_1 = f_{e1}$, $f_p = \sqrt{f_{e2}^2 + f_{e3}^2}$).

Fig. 9. Screw-driver operation about the N-axis with $\psi_d(t) := \psi_{\max} \sin \omega_n t$ and $\psi_d(t) := \psi_{\max} \sin(\omega_n/2)t$.

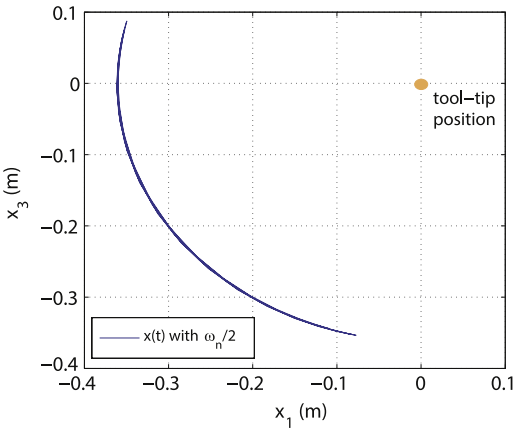

(a) Trajectory of the quadrotor center-of-mass position x (positive x_3 implies downward direction).

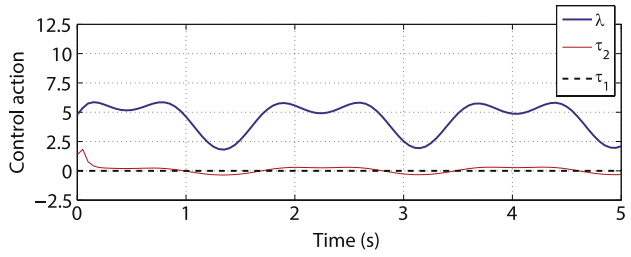

(b) Control action λ, τ.

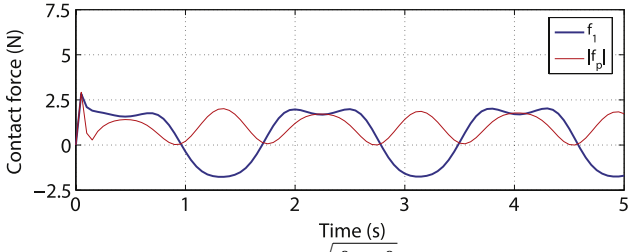

(c) Contact force f_e (with $f_1 = f_{e1}$, $f_p = \sqrt{f_{e2}^2 + f_{e3}^2}$).

Fig. 10. Vertical jack operation about the E-axis with $\theta_d(t) := \theta_{\max} \sin \omega_n t$.

this, we apply the ν_3-action (16), which turns out to be crucial here, as it can prevent finite-time escape of the internal dynamics (11) even against the sudden surges of angular rate ω due to the tool–surface collision impacts (even with $d_3 < 0$—see Fig. 11) or aggressive transition from the unstable equilibrium to the stable equilibrium with $d_3 > 0$ (see Fig. 12). If it were not for this ν_3-action, these sudden surges of w would trigger finite-time escape, thereby, invalidate the dynamics (26).

As stated after Theorem 3 of Section 3.3, this ν_3-action does not at all interfere with the tool-tip control u, implying that, here, we can just focus on the design of u in (26). This ν_3-action, as also mentioned in Section 3.3, yet, can produce extra rotation motion, which may induce quadrotor–surface collision. Although no collision occurs here in our simulation, how to prevent collision, or, even further, how to achieve collision avoidance ability, by exploiting this ν_3-action is a topic of our on-going work (see the second last paragraph of Section 3.3).

With this stabilizing, yet, decoupled ν_3-action, we can then just focus on (26) to design the hybrid position/force control for u. For this, we particularly utilize passive decomposition (Lee, 2010; Lee & Li, 2013), which not only provides both the tangential and normal dynamics w.r.t. the surface (in contrast to Murray, Li, & Sastry, 1993), but also requires less cancellation of the open-loop dynamics (as compared to Khatib, 1987). A full treatment of general hybrid position/force control is not a main topic of this paper and we refer readers to the above references.

We first define the two-dimensional working surface of the tool-tip $y \in \Re^3$ by

$$h(y) = 0 \tag{27}$$

where $h : \Re^3 \to \Re$ is a smooth function with the full-rank Jacobian, with its level sets constituting a foliation of the working surface. Then, following (Lee & Li, 2013), at each y, we can decompose the tangent space $T_y\mathcal{M}$ and the cotangent space $T_y^*\mathcal{M}$ of the y-dynamics (26) s.t.,

$$T_q\mathcal{M} = \mathcal{D}^\top \oplus \mathcal{D}^\perp \quad \text{and} \quad T_q^*\mathcal{M} = \Omega^\top \oplus \Omega^\perp$$

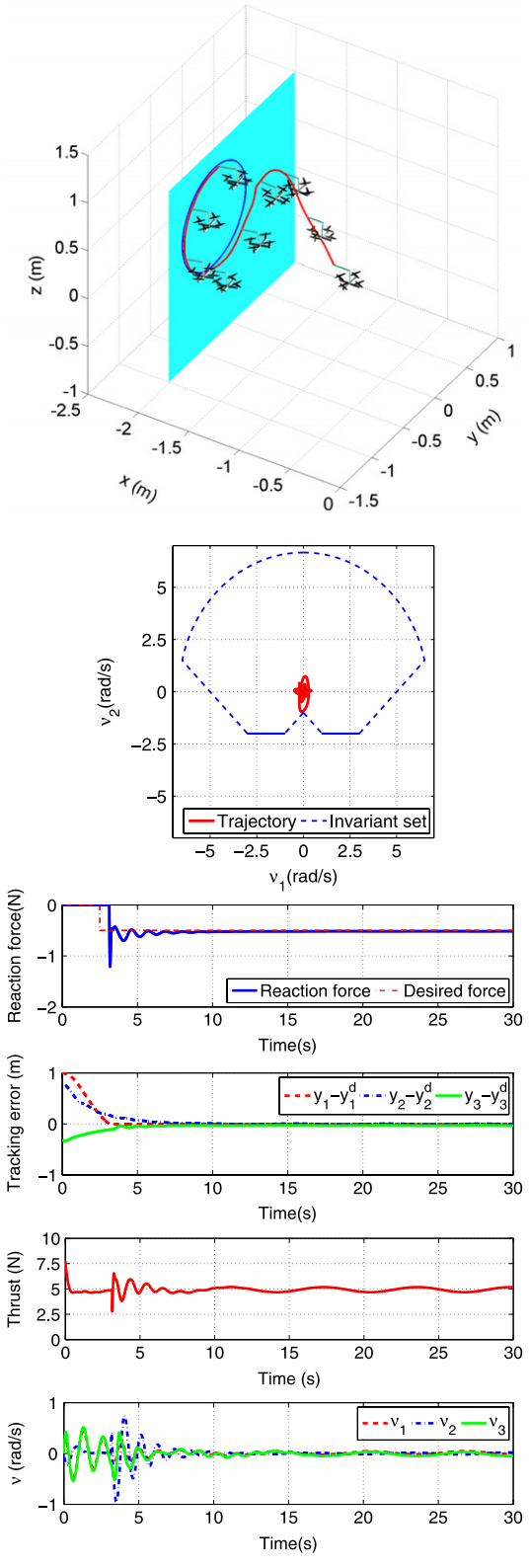

Fig. 11. Hybrid position/force control with $d = [0.35; 0; -0.3]$ m and the stabilizing ν_3-action (16).

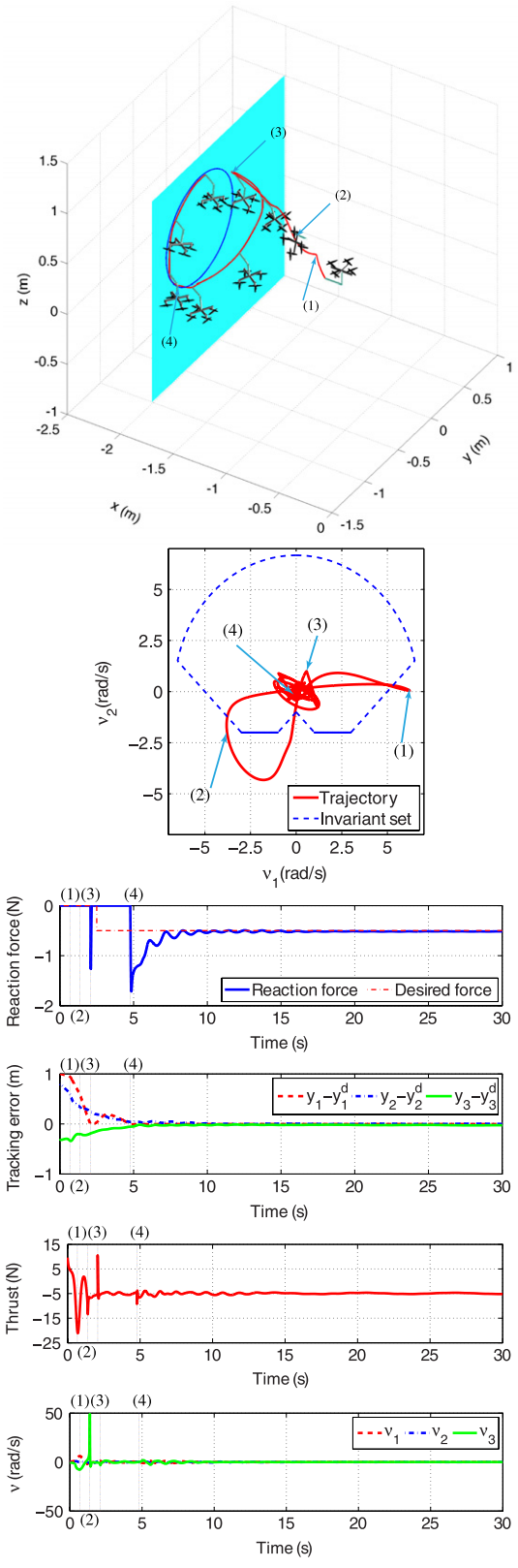

Fig. 12. Hybrid position/force control with $d = [0.35; 0; 0.3]$ m and the stabilizing ν_3-action (16).

where $\mathcal{D}^{\top}$ and $\mathcal{D}^{\perp}$ are the distributions of the null-space of $\frac{\partial h}{\partial y}$ and the orthogonal complement of $\mathcal{D}^{\top}$ w.r.t. the inertia metric m of (26); and $\Omega^{\top}$ and $\Omega^{\perp}$ are the annihilating co-distributions of $\mathcal{D}^{\perp}$ and $\mathcal{D}^{\top}$, respectively.

With this decomposition of the tangent and co-tangent spaces, we can write the velocity $\dot{y}$ and control/contact-force $u + f_e$ of the y-dynamics (26) s.t.,

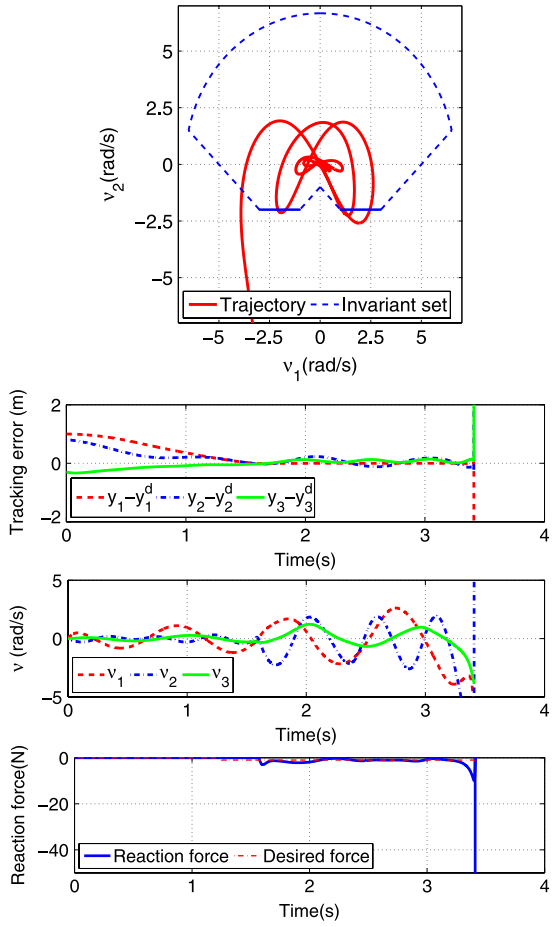

Fig. 13. Hybrid position/force control with $d = [0.35; 0; -0.3]$ m and the v_3-action (16) deactivated.

$$\dot{y} =: \underbrace{\begin{bmatrix}\mathcal{D}_\top & \mathcal{D}_\perp\end{bmatrix}}_{=:\mathcal{D}(y)} \begin{pmatrix} v_l \\ v_h \end{pmatrix},$$
$$u + f_e =: \underbrace{\begin{bmatrix}\Omega_\top^T & \Omega_\perp^T\end{bmatrix}}_{=:\Omega^T(y)} \begin{pmatrix} u_l + f_l \\ u_h + f_h \end{pmatrix} \tag{28}$$

where $v := [v_l; v_h] \in \Re^3$ is the transformed velocity, and the matrices $\mathcal{D}_\top \in \Re^{3\times 2}$, $\mathcal{D}_\perp \in \Re^{3\times 1}$, $\Omega_\top \in \Re^{2\times 3}$ and $\Omega_\perp \in \Re^{1\times 3}$ identify $\mathcal{D}^\top$, $\mathcal{D}^\perp$, $\Omega^\top$ and $\Omega^\perp$, respectively. Since the inertia metric m of (26) is Euclidean, following (Lee & Li, 2013), we can obtain the following closed-form expressions for these matrices: $\mathcal{D}_\top \approx \text{null}(\partial h/\partial y)$ with $\mathcal{D}_\top^T \mathcal{D}_\top = I$, $\Omega_\perp = \frac{\partial h}{\partial y}$, $\mathcal{D}_\perp = \Omega_\perp^T(\Omega_\perp \Omega_\perp^T)^{-1}$, and $\Omega_\top = (\mathcal{D}_\top^T \mathcal{D}_\top)^{-1}\mathcal{D}_\top^T$. We can then show that

$$\mathcal{D}_\top^T \mathcal{D}_\perp = 0, \qquad \Omega \mathcal{D} = I, \qquad \frac{dh}{dt} = \Omega_\perp \dot{y} = \Omega_\perp \mathcal{D}_\perp v_h = v_h$$

where the last equation clearly shows that $v_h \in \Re$ is the velocity of the tool-tip y normal to the working surface, while $v_l \in \Re^2$ is the tangential to the surface.

Differentiating (28), we can further obtain

$$\ddot{y} = \mathcal{D}\dot{v} + \dot{\mathcal{D}} v$$

and, inserting this into (26) with the left-multiplication by $\mathcal{D}^T$, we can achieve

$$m\dot{v}_l + Q_l(y,\dot{y})v_l + Q_{lh}(y,\dot{y})v_h = u_l + f_l \tag{29}$$
$$m\dot{v}_h + Q_h(y,\dot{y})v_h + Q_{hl}(y,\dot{y})v_l = u_h + f_h \tag{30}$$

where $v_h = \dot{h}$ and

$$m\mathcal{D}^T(y)\dot{\mathcal{D}}(y) =: \begin{bmatrix} Q_l(y,\dot{y}) & Q_{lh}(y,\dot{y}) \\ Q_{hl}(y,\dot{y}) & Q_h(y,\dot{y}) \end{bmatrix}.$$

The dynamics in (29) is called *locked system*, which specifies the y-dynamics tangential to the working surface (27), whereas the dynamics in (30) *shape system*, which describes the y-dynamics normal to the surface (27). Both of these locked and shape systems inherit the Lagrange structure and passivity from the original dynamics (26), with $Q_l \in \Re^{2\times 2}$ being skew-symmetric, $Q_h = 0$ and $Q_{lh}^T = -Q_{hl}$. This preserved structure and passivity can be utilized for control synthesis (e.g., passivity-based control) as shown below. For more details on passive decomposition, refer to (Lee, 2010; Lee & Li, 2013).

Once we have the locked-shape dynamics decomposition (29)–(30), it becomes rather straightforward to design the hybrid position/force control. First, to drive the tool-tip position y on the working surface (27), we can control the locked system (29). For this, denote a local parameterization of the surface by $q_l := q_l(y) \in \Re^2$. Differentiating q_l with the fact that $q_l(y)$ does not change along the normal direction to the surface, we then have

$$\dot{q}_l := \frac{\partial q_l}{\partial y}\dot{y} = \frac{\partial q_l}{\partial y}\mathcal{D}_\top v_l =: B^{-1}(y) v_l$$

where $B(y) := \left(\frac{\partial q_l}{\partial y}\mathcal{D}_\top\right)^{-1} \in \Re^{2\times 2}$ is assumed to exist locally. With this B, we can further obtain that $v_l = B\dot{q}_l$ and $\dot{v}_l = B\ddot{q}_l + \dot{B}\dot{q}_l$, and, substituting these to (29) and left multiplying by B^T, we have

$$mB^T B\ddot{q}_l + B^T(m\dot{B} + Q_l B)\dot{q}_l + B^T Q_{lh} v_h = B^T(u_l + f_l)$$

where $mB^T B \in \Re^{2\times 2}$ is the positive-definite projected inertia on the surface with $\frac{d}{dt}(mB^T B) - 2B^T(m\dot{B} + Q_l B)$ being skew-symmetric. We can then design the following exponentially-converging passivity-based tracking control on the surface:

$$u_l := Q_{lh}v_h - f_l + mB\ddot{q}_l^d + (m\dot{B} + Q_l B)\dot{q}_l^d - B^{-T}[b_l(\dot{q}_l - \dot{q}_l^d) + k_l(q_l - q_l^d)] \tag{31}$$

where $b_l, k_l > 0$ are the control gains, and $q_l^d(t) \in \Re^2$ is the desired trajectory on the surface.

On the other hand, for the tool-tip behavior normal to the surface, we can control the shape system (30). For this, when y is outside the surface, we first apply the following control u_l to approach to the surface:

$$u_h := Q_{lh}v_l - b_h v_h - k_h(h - h^\star) \tag{32}$$

where $v_h = \dot{h}$, $Q_h = 0$ and $h^\star \in \Re$ is the set-position slightly within (or close to) the surface (27), and k_v, $k_p > 0$ are the control gains. Once contact is detected, we then switch to the following normal force control:

$$u_h := Q_{lh}v_l - b_h v_h - f_h^d - k_i \int_0^t (f_h^d - f_h)ds \tag{33}$$

where $f_h^d \in \Re$ is the desired contact force, and $b_h, k_i > 0$ are the control gains. See (Tarn, Wu, Xi, & Isidori, 1996) for some gain conditions, with which we can ensure $f_h \to f_h^d$ after only a finite number of switchings between these controls u_h.

This designed hybrid position/force control (u_l, u_h) is then decoded into the control inputs (λ, τ) of the quadrotor (1)–(2) as follows: (1) transform (u_l, u_h) back to the desired tool-tip control u by (28); (2) compute the thrust input λ and the desired $(\dot{v}_1, \dot{v}_2)$ to produce this u from the internal dynamics (9); (3) given $(\dot{v}_1, \dot{v}_2)$ and the $\dot{v}_3$-action of (16), obtain the desired angular acceleration $\dot{\omega}^d \in \Re^3$ by using (8); and (4) compute the torque input τ via (7) to achieve $\dot{\omega} \to \dot{\omega}^d$. The following Theorem 4 summarizes main property of the hybrid position/force control (31)–(33), for which the decoupling between the v_3-action and the generation of u via (9) is crucial.

Theorem 4. *Consider the quadrotor-tool system (1)–(2) under the hybrid position/force control (31)–(33) and the ν_3-action (16). Then, $q_l \to q_l^d$ exponentially and $f_h \to f_h^d$ asymptotically (under the condition of Tarn et al., 1996) without finite-time escape of internal dynamics.*

We perform simulations of this hybrid position/force control. For that, we assume 2% of parametric uncertainty and 3% actuation uncertainty. We approximate the discontinuous sgn(·) function by the continuous atan(·) function for the ν_3-action (16) as mentioned in Section 3.3. We define the working surface to be a vertical plane defined by $x = -2$ [m] as shown in Fig. 11.

For the first simulation, we set $d = [0.35; 0; -0.3]$ m (i.e., tool above the quadrotor) according to Theorem 2 to maintain the stable tool operation configuration. We also activate the ν_3-action (16) to prevent finite-time escape according to Theorem 3. The results are shown in Fig. 11, where we can observe that, even with the surge of angular velocity due the impact between the tool-tip and the surface (around 3 s), the quadrotor can still maintain stable operation thanks to the stabilizing ν_3-action, with which (ν_1, ν_2) can stay within the compact set $\mathcal{S}$ of Theorem 3 (second plot of Fig. 11). We can also see from Fig. 11 that the trajectory tracking can be ensured even during the impact (with no limit imposed on the control λ, τ) and also with the ν_3-action (see the last third paragraph of Section 3.3). The contact force control is also decoupled from the ν_3-action as well, which is yet difficult to see from Fig. 11, as the transient behavior of the contact force control after the impact excites the ν_3-action (16).

For the second simulation, we set $d = [0.35; 0; 0.3]$ m to intentionally violate the necessary condition of Theorem 2, yet, still keep the ν_3-action of Theorem 3. The results are presented in Fig. 12, where we can observe that, as the quadrotor starts from the unstable configuration (i.e., with the tool below it), it is flipping over by itself to the stable equilibrium (i.e., tool above the quadrotor). It also hits the wall around 2 s, (indicator (3) of Fig. 12) with a large impact force, bounces back from the wall, approaches and makes a contact with the wall again around 5 s (indicator (4)). After that, the quadrotor attains the steady-state trajectory tracking and the normal force regulation while maintaining the stable posture (i.e., tool above the quadrotor).

During the course of flipping (indicator (2) in Fig. 12) and also after the impacts, the quadrotor gains fairly large angular velocity, which is then suppressed by the ν_3-action not to trigger finite-time escape. Similar to Fig. 11, in Fig. 12, both the trajectory tracking and the contact force control are achieved without being affected by the ν_3-action, with the first even ensured during the impacts as well. It is also worthwhile to mention that the indicators (1) and (2) outside the invariant set $\mathcal{S}$ in Fig. 12 do not contradict to Theorem 3, as the invariant set $\mathcal{S}$ in Theorem 3 is defined for the stable posture (i.e., tool above the quadrotor), yet, the indicators (1) and (2) of Fig. 12 are associated when the quadrotor is operating around the unstable equilibrium (i.e., tool below the quadrotor).

We also perform the simulation with the same setting as Fig. 11, yet, in this case, turn off the ν_3-action. The results are shown in Fig. 13, where we can see that, even if the necessary condition of Theorem 2 is granted, without the ν_3-action, the sudden increase of the angular velocity when the quadrotor hits the wall (around 3 s both for Figs. 11 and 13) indeed triggers finite-time escape. We observe similar occurrence of the finite-time escape when we turn off the ν_3-action for the simulation of Fig. 12 (not shown here), for which finite-time escape occurs as the quadrotor is flipping over (i.e., indicator (2) of Fig. 12).

5. Summary and future work

In this paper, we investigate issues salient to the dynamics and control of the quadrotor, when it is operating a simple rigid tool attached on it. Some structural conditions are elucidated to generate arbitrary tool-tip Cartesian control action (Theorem 1) and also to avoid instability of the internal dynamics (Theorem 2), which inevitably arises due to the quadrotor's under-actuation. This necessary condition for the internal stability (Theorem 2) is particularly interesting, since it suggests a design, which would appear counter-intuitive to the practitioners, that is, the tool should be installed above the quadrotor, not below it. We also fully characterize the four-dimensional nonlinear internal dynamics of the spatial quadrotor tool-operation, manifest that some quadratic terms therein can trigger finite-time escape, and propose a stabilizing control action to suppress that (Theorem 3). The obtained theoretical results are then illustrated/validated for the two practically-important application scenarios: (1) rotational tool operation including screw-driver and vertical-jack; and (2) hybrid position/force control against a working surface.

On-going and possible future research topics include: (1) experimental verification of the proposed framework, particularly relying on on-board sensors; (2) incorporation of collision avoidance ability into our framework, particularly via state-dependent switching ν_3-action; and (3) cooperation of multiple quadrotor-tool systems and their teleoperation.

References

Abdessameud, A., & Tayebi, A. (2010). Formation control of vtol uavs without linear-velocity measurements. In *Proc. American control conference* (pp. 2107–2112).

Aguiar, A. P., & Hespanha, J. P. (2007). Trajectory-tracking and path-following of underactuated autonomous vehicles with parametric modeling uncertainty. *IEEE Transactions on Automatic Control*, *52*(8), 1362–1379.

Bellens, S., De Schutter, J., & Bruyninckx, H. (2012). A hybrid pose/wrench control framework for quadrotor helicopters. In *Proc. IEEE int'l conference on robotics & automation* (pp. 2269–2274).

Brescianini, D., Hehn, M., & D'Andrea, R. (2013). Quadrocopter pole acrobatics. In Proc. IEEE/RSJ int'l conf. intelligent robots & systems (pp. 3472–3479).

Darivianakis, G., Alexis, K., Burri, M., & Siegwart, R. (2014). Hybrid predictive control for aerial robotic physical interaction towards inspection operations. In *Proc. IEEE/RSJ int'l conf. intelligent robots & systems* (pp. 53–58).

Franchi, A., Secchi, C., Son, H.-I., Bulthoff, H. H., & Robuffo, P. (2012). Giordano. Bilateral teleoperation of groups of mobile robots with time-varying topology. *IEEE Transactions on Robotics*, *28*(5), 1019–1033.

Frazzoli, E., Dahleh, M. A., & Feron, E. (2000). Trajectory tracking control design for autonomous helicopters using a backstepping algorithm. In *Proc. American control conference* (pp. 4102–4107).

Getz, W. M., & Jacobson, D. H. (1977). Sufficiency conditions for finite escape times in systems of quadratic differential equations. *IMA Journal of Applied Mathematics*, *19*(4), 377–383.

Ghadiok, V., Goldin, J., & Ren, W. (2012). On the design and development of attitude stabilization, vision-based navigation, and aerial gripping for a low-cost quadrotor. *Autonomous Robots*, *33*, 41–68.

Ha, C., Zuo, Z., Choi, F. B., & Lee, D. J. (2014). Passivity-based adaptive backstepping control of quadrotor-type uavs. *Robotics & Autonomous Systems*, *62*(9), 1305–1315.

Hauser, J., Sastry, S., & Meyer, G. (1992). Nonlinear control design for slightly non-minimum phase systems: application to v/stol aircraft. *Automatica*, *28*(4), 665–679.

Hehn, M., & D'Andrea, R. (2011). A flying inverted pendulum. In *Proc. IEEE int'l conference on robotics & automation* (pp. 763–770).

Hua, M.-D., Hamel, T., Morin, P., & Samson, C. (2009). A control approach for thrust-propelled underactuated vehicles and its application to vtol drones. *IEEE Transactions on Automatic Control*, *54*(8), 1837–1853.

Khatib, O. (1987). A unified approach for motion and force control of robot manipulators: the operational space formulation. *IEEE Journal of Robotics & Automation*, *RA-3*(1), 43–53.

Korpela, C., Orsag, M., Oh, P., & Pekala, M. (2013). Dynamic stability of a mobile manipulating unmanned aerial vehicle. In *Proc. IEEE int'l conference on robotics & automation* (pp. 4907–4912).

Lee, D. J. (2010). Passive decomposition and control of nonholonomic mechanical systems. *IEEE Transactions on Robotics*, *26*(6), 978–992.

Lee, D. J. (2012). Distributed backstepping control of multiple thrust-propelled vehicles on a balanced graph. *Automatica*, *48*(11), 2971–2977.

Lee, D. J., Franchi, A., Son, H.-I., Ha, C., Bülthoff, H. H., & Robuffo Giordano, P. (2013). Semi-autonomous haptic teleoperation control architecture of multiple unmanned aerial vehicles. *IEEE/ASME Transactions on Mechatronics*, *18*(4), 1334–1345.
Lee, D.J., & Ha, C. (2012). Mechanics and control of quadrotor for tool operation. In *Proc. ASME dynamic systems & control conference* (pp. 177–184).
Lee, D. J., & Li, P. Y. (2013). Passive decomposition of multiple mechanical systems under motion coordination requirements. *IEEE Transactions on Automatic Control*, *58*(1), 230–235.
Marconi, L., & Naldi, R. (2012). Control of aerial robots: Hybrid force and position feedback for a ducted fan. *IEEE Control Systems Magazine*, *32*(4), 43–65.
Martin, P., Devasia, S., & Paden, B. (1996). A different look at output tracking: control of a vtol aircraft. *Automatica*, *32*(1), 101–107.
Mellinger, D., Michael, N., & Kumar, V. (2012). Trajectory generation and control for precise aggressive maneuvers with quadrotors. *International Journal of Robotics Research*, *31*(5), 664–674.
Murray, R. M., Li, Z., & Sastry, S. S. (1993). *A mathematical introduction to robotic manipulation*. Boca Raton, FL: CRC.
Nguyen, H.-N., & Lee, D. J. (2013). Hybrid force/motion control and internal dynamics of quadrotors for tool operation. In *Proc. IEEE/RSJ int'l conference on intelligent robots & systems* (pp. 3458–3464).
Palunko, I., & Fierro, R. (2011). Adaptive control of a quadrotor with dynamic changes in the center of gravity. In *Proc. of IFAC world congress, Vol. 18* (pp. 2626–2631).
Pounds, P. E., Bersak, D. R., & Dollar, A. M. (2012). Stability of small-scale UAV helicopters and quadrotors with added payload mass under PID control. *Autonomous Robots*, *33*(1–2), 129–142.
Purwin, O., & D'Andrea, R. (2009). Performing aggressive maneuvers using iterative learning control. In *Proc. IEEE int'l conference on robotics & automation* (pp. 1731–1736).
Sepulchre, R., Jankovic, M., & Kokotovic, P. (1997). *Constructive nonlinear control*. London: Springer-Verlag.
Slotine, J.-J. E., & Li, W. (1991). *Applied nonlinear control*. Englewood Cliffs, NJ: Prentice Hall.
Spong, M. W., Hutchinson, S., & Vidyasaga, M. (2006). *Robot modeling and control*. Hoboken, NJ: John Wiley & Sons.
Tarn, T. J., Wu, Y., Xi, N., & Isidori, A. (1996). Force regulation and contact transition control. *IEEE Control Systems Magazine*, *16*(1), 32–40.
Turpin, M., Michael, N., & Kumar, V. (2012). Trajectory design and control for aggressive formation flight with quadrotors. *Autonomous Robots*, *33*(1–2), 143–156.
Yang, H., & Lee, D. J. (2014). Dynamics and control of quadrotor with robotic manipulator. In *Proc. IEEE int'l conference on robotics & automation* (pp. 5544–5549).

Hai-Nguyen Nguyen received the B.S. degree in Mechatronics and the M.S. degree in Applied Mechanics from the Hanoi University of Science & Technology, Vietnam, 2008 and 2010. From 2009 to 2012, he was a permanent researcher with the Institute of Mechanics, Vietnam Academy of Science & Technology. He is currently working toward the Ph.D. degree in Mechanical Engineering at Seoul National University. He research interests include dynamics and control problems related to aerial manipulation.

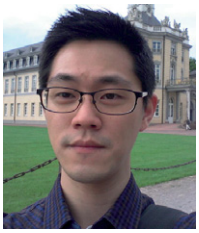

ChangSu Ha received the B.S. degree from the Sungkyunkwan University, Suwon, Korea, 2002, and the M.S. degree from the Seoul National University (SNU), Seoul, Korea, 2013, both in Mechanical Engineering. He is currently working toward his Ph.D. degree in Mechanical Engineering at the Seoul National University. His research interests include teleoperation and control of mobile robots.

Dongjun Lee is an Associate Professor with the Department of Mechanical & Aerospace Engineering at the Seoul National University. He received the B.S. and M.S. degrees from KAIST, Korea, and the Ph.D. degree in Mechanical engineering from the University of Minnesota, respectively in 1995, 1997 and 2004. He was an Assistant Professor with the Department of Mechanical, Aerospace & Biomedical Engineering at the University of Tennessee, 2006–2011, and a Postdoctoral Researcher with the Coordinated Science Laboratory at the University of Illinois at Urbana–Champaign, 2004–2006. His main research interests are dynamics and control of robotic and mechatronic systems with emphasis on teleoperation/haptics, multirobot systems, aerial robots, and geometric mechanics control theory. Dr. Lee received the US NSF CAREER Award in 2009, the Best Paper Award from the IAS-2012, and the 2002–2003 Doctoral Dissertation Fellowship of the University of Minnesota. He was an Associate Editor of the IEEE Transactions on Robotics.